第35卷 第3期 焊 接 学 报 Vol. 35 No. 3
2014年3月 TRANSACTIONS OF THE CHINA WELDING INSTITUTION March 2014

搅拌摩擦焊过程中搅拌头温度场分布特征

李敬勇， 赵阳阳， 亓晓亮
(江苏科技大学 先进焊接技术省级重点实验室，镇江 212003)

摘 要：试验测定了搅拌头温度分布曲线，分析了搅拌头温度场的分布特征，对比研究了不同材质搅拌头温度分布的特点. 结果表明，摩擦焊初始阶段，搅拌区域金属的软化致使摩擦针与试板之间的摩擦产热量降低，在搅拌头轴肩与试板接触之前，搅拌头温度出现滞涨，并出现一定程度的回落；稳定焊接阶段，摩擦热传递至搅拌头的热量与通过其散失的热量处于动平衡状态，其温度波动较小；高速旋转搅拌头的表面与周围空气进行强烈的热交换，搅拌头轴线上的温度高于外缘的温度；采用比热容小、热导率高材质制作的搅拌头，焊接过程中其温度变化快，整体温度高.

关键词：搅拌摩擦焊； 搅拌头； 温度场
中图分类号：TG455 **文献标识码**：A **文章编号**：0253－360X(2014)03－0066－05

0 序 言

搅拌摩擦焊通过摩擦产生的热量仅能使被焊金属达到塑态[1]，因此在实现易于受焊接热循环影响材料的连接时，在焊接接头力学性能、焊接区域的应力状态及焊接连接的可实现性等方面均表现显著优势[2]. 搅拌摩擦焊热过程一直是国内外焊接界研究的热点之一[3－8]. 通过对搅拌摩擦焊热过程的深入了解，可以预测焊接过程中的温度、应力和应变的分布，以及接头区域的微观特征，进而评价接头性能. 掌握搅拌摩擦焊接过程的温度分布，可以更好地计算与搅拌摩擦焊流场计算密切相关的材料黏度等特性，从而为深入研究焊接过程中材料的流场分布规律奠定基础.

搅拌头是搅拌摩擦焊的“心脏”[9]，它既是完成搅拌摩擦焊过程必不可少的产热工具，同时也是焊接热量散失的主要途径. 掌握搅拌头的温度场分布信息有助于了解整个焊接热过程、分析焊接残余应力的分布和残余变形的状态、研究接头微观组织演变、优化焊接工具的选材和设计. 目前大部分试验研究均是在焊接工件中插入热电偶测量温度场的分布，即主要测定搅拌摩擦焊过程中焊接试样的温度分布情况[10]，而对于搅拌工具的温度场分布则鲜见报道. 文中应用热电偶测温技术和自行研制的无线测温系统，通过试验方法测定了不同边界条件下的搅拌头温度场的分布规律，从而为全面了解搅拌摩擦焊热过程规律奠定了基础，文中主要介绍搅拌头的温度场分布特征，并初步分析了搅拌头材质对其温度场的影响.

1 搅拌头温度场的试验测定

目前铝合金焊接常用搅拌头的材质有工具钢、模具钢及不锈钢等. 文中主要选择高速工具钢W9Mo3Cr4V做铝合金搅拌摩擦焊工具的制作材料，铝与W9Mo3Cr4V的摩擦产热量比较高，可以使焊接速度提高或者降低搅拌头的旋转频率，最大限度的提高生产效率. 作为对比研究，还采用SUS440C马氏体不锈钢搅拌头进行了相同参数下铝合金的搅拌摩擦焊. 表1和表2分别列出了两种材料的化学成分.

表1 高速钢W9Mo3Cr4V化学成分(质量分数，%)
Table 1 Chemical compositions of red-hard steel W9Mo3Cr4V

C	W	Mo	Cr	V	Si	Mn	S	P
0.77～0.87	8.50～9.50	2.70～3.30	3.80～4.40	1.30～1.70	0.20～0.40	0.20～0.40	≤0.03	≤0.03

收稿日期：2013－05－08
基金项目：西北工业大学陕西省摩擦焊重点实验室基金资助项目(SHAANXI-KL-FW-201002)；江苏高校优势学科建设工程资助项目(PDAD)

为了测定搅拌头温度场，考虑到搅拌头开孔对其散热条件及强度的影响，选择在搅拌头不同的横

表 2　不锈钢 SUS440C 化学成分(质量分数，%)

Table 2　Chemical compositions of stainless steel SUS440C

C	Si	Mn	Cr	Mo	S	P
0.95～1.20	1.00	1.00	16.0～18.0	0.75	0.03	0.04

截面上开不同深度的孔，孔底即为搅拌头测温特征点. 测温采用直径为 ϕ 1 mm 的铠装热电偶，测温孔径为 ϕ 1.2 mm. 试验过程中热电偶插入测温孔中，随搅拌头高速旋转，通过自行研制的无线测温系统和接收装置，将特征点的实时温度传送至与接收装置连接的计算机. 搅拌头测温点的分布如图 1 所示. 搅拌头测温孔在垂直于其轴线的投影面上分别呈 120°夹角分布. 为了更清楚地描述搅拌头测温特征点的位置，依次将从轴肩向远离试板平面的特征点称为 CH003，CH002 和 CH001.

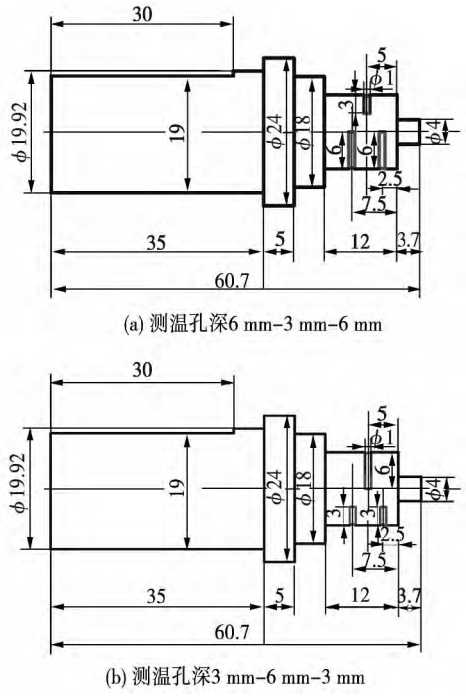

图 1　搅拌头打孔位置及尺寸示意图(mm)

Fig. 1　Schematic diagram of points' distribution for measuring temperature in stirring tools

焊接试验利用 FSW-3LM-002 型数控搅拌摩擦焊机，试验材料为 5A15 铝合金，其化学成分列于表 3. 焊接试板尺寸为 140 mm×40 mm×4 mm. 焊接参数为旋转频率 1 500 r/min，焊接速度 25 mm/min，焊接倾角 2.5°，达到下压量设置值停留 8 s 后，搅拌头再向前移动实现焊接过程. 搅拌头测温系统采样频率为 1 Hz.

表 3　5A15 铝合金材料的化学成分(质量分数，%)

Table 3　Chemical compositions of aluminum alloy 5A15

Mn	Si	Cu	Cr	Zn	Fe	Mg	Ti	其它	Al
0.4～1.0	0.40	0.10	0.05～0.25	0.25	0.40	4.0～4.9	0.15	0.15	余量

2　搅拌头温度变化曲线

试验测量结果显示，搅拌头各特征点温度变化曲线如图 2 所示. 由图 2 发现，搅拌摩擦焊接过程主要分为三个阶段：搅拌头插入试板阶段、摩擦稳定焊接阶段及搅拌头升出阶段. 在搅拌针插入阶段(图 2 中 A 段)，搅拌头各特征点的温度明显升高，因为随着搅拌针逐渐插入，其与试板的有效摩擦面不断增大，导致摩擦产热量增大；同时搅拌头测温点与摩擦产热界面的距离越来越近，导致测温点的温度持续升高；在摩擦稳定焊接阶段(图 2 中 D 段)，轴肩及搅拌针与焊接试板之间摩擦产热一方面使试板加热塑化，产生塑性流动，另一方面热量通过试板和搅拌工具散失，使搅拌头温度处于准稳态状态，温度变化不明显；在搅拌摩擦焊过程完成、搅拌头升出阶段(图 2 中 E 段)，摩擦产热逐渐消失，搅拌头的温度则迅速降低.

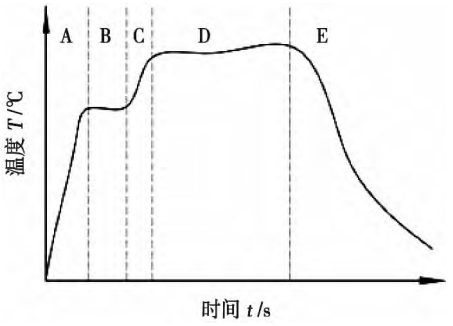

图 2　搅拌摩擦焊各阶段温度示意图

Fig. 2　Schematic diagram of temperature-time curve of stirring tool

在搅拌头插入阶段和稳定摩擦焊接阶段之间，搅拌头温度曲线上出现一个“平台”(图 2 中 B 段)，即在这段时间内，搅拌头温度没有继续升高，甚至还出现一定程度的回落. 产生此现象的原因主要是随着搅拌针的逐渐插入，其与焊接试板之间产生的摩擦热使搅拌针周围的金属逐渐软化成塑态，软化金属与搅拌针之间的摩擦系数减小，从而导致摩擦产热量大大降低，这样搅拌头的温度不仅不能持续升高，搅拌头靠近轴肩平面的区域，由于其散热条件相对较好，其温度反而还会出现一定程度的回落. 当轴肩接触到焊接试板，高速旋转的轴肩平面与试板摩擦产生大量热，致使搅拌摩擦偶温度再次升高

(图 2 中 C 段),试板搅拌区域进一步软化. 随后搅拌头向前移动实现搅拌摩擦焊过程. 由于搅拌针周围金属一直处于软化状态,因此轴肩与焊接试板之间的摩擦热逐渐成为搅拌摩擦焊接过程的主要热源.

3 搅拌头温度场的分布特征

图 3a,b 是分别采用图 1a,b 所示搅拌头测温孔分布时,焊接过程中高速工具钢搅拌头各特征点的温度变化曲线,稳定焊接阶段搅拌头的温度变化范围列于表 4,并图示于图 4.

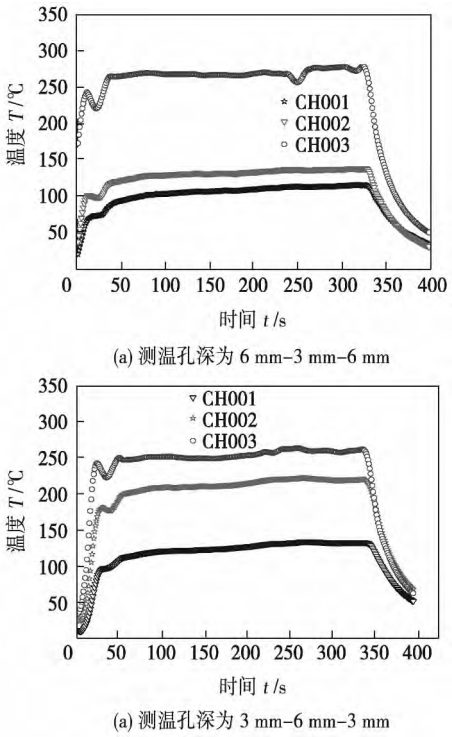

图 3 不同孔深的搅拌头特征点温度曲线

Fig. 3 Temperature-time curves of red-hard steel tool

表 4 焊接平稳阶段不同材质搅拌头各特征点温度波动范围

Table 4 Temperature fluctuation ranges in stirring tools made of W9Mo3Cr4V and SUS440C

搅拌头材质	特征点温度波动范围 T/℃			特征点径向分布特征
	CH001	CH002	CH003	
W9Mo3Cr4V	93 ~ 116	121 ~ 139	264 ~ 280	6 mm-3 mm-6 mm
W9Mo3Cr4V	110 ~ 130	197 ~ 215	245 ~ 260	3 mm-6 mm-3 mm
SUS440C	92 ~ 112	145 ~ 165	237 ~ 261	6 mm-3 mm-6 mm
SUS440C	93 ~ 116	174 ~ 192	189 ~ 200	3 mm-6 mm-3 mm

由表 4 及图 4 可以看出,靠近搅拌头轴肩摩擦面测温点温度最高,随着测温特征点远离摩擦产热面,其温度逐渐降低. 同一层测温平面上,搅拌头轴

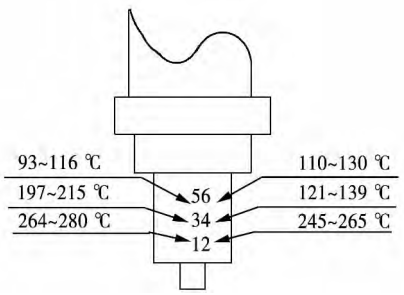

图 4 高速钢圆柱针形搅拌头特征点温度波动范围

Fig. 4 Temperature distributions in cylindrical red-hard steel tool

线上测温点 1 和 3 的温度均高于 1/2 半径处测温点 2 和 4 的温度. 在多数搅拌摩擦焊数值模拟分析中,摩擦面热源模型均阐述为热流密度与离轴线的距离成反比关系,认为越远离轴心的点,其线速度越大,搅拌头与试板之间摩擦越剧烈,产生的热量越多,越靠近搅拌头轴肩外缘,其温度值越高. 上述结论显然忽略了热量的累积效应. 随着搅拌针持续插入焊接试板,及搅拌头轴肩与试板接触,搅拌头与试板之间摩擦产生的热量,一方面传递至试板,使试板温度升高并软化,在搅拌针及轴肩的机械作用下,实现搅拌摩擦焊缝的形成; 另一方面持续传递至搅拌头,使搅拌头温度升高. 摩擦热一方面通过搅拌头自身热传导散失,同时高速旋转的搅拌头还与周围空气进行强烈的对流和辐射热交换. 搅拌头表面与空气直接接触,热交换更为充分,因此通过搅拌头表面散失了热量较其轴心区域更多,从而出现了在搅拌头同一测温平面上,从轴线向外缘温度递减的分布特征. 适当的焊接参数条件下,搅拌摩擦偶产生并传递至搅拌头的热量与搅拌头通过传导、对流及辐射散失的热量达到动态平衡时,搅拌头各测温点的温度基本保持不变,即达到搅拌摩擦焊的稳定焊接阶段.

4 材质对搅拌头温度场分布的影响

图 5 为采用图 1b 所示搅拌头测温孔时,焊接过程中 SUS440C 搅拌头各特征点的温度变化曲线. 焊接稳定阶段其温度变化范围也列于表 4. 图 6 为焊接稳定阶段不锈钢搅拌头各特征点的温度变化范围. 由图 6 及表 4 可以看出,不锈钢搅拌头温度场的分布具有与高速工具钢搅拌头同样的规律,即搅拌头轴线上测温点的温度均高于 1/2 半径处测温点温度.

对比图 4 与图 6 发现,在同样焊接条件下,高速工具钢搅拌头各测温点的温度均高于不锈钢搅拌头

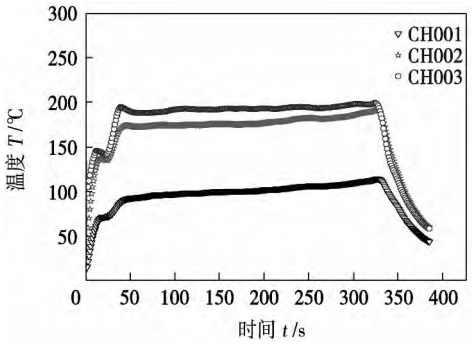

图 5　不锈钢搅拌头温度变化曲线

Fig. 5　Temperature-time curve of stainless steel tool

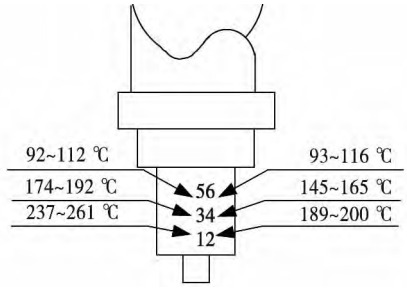

图 6　不锈钢圆柱针形搅拌头特征点温度波动范围

Fig. 6　Temperature distributions in cylindrical stainless steel tool

对应测温点的温度. 越靠近轴肩摩擦面测温点，其温差越大.

表 5 为搅拌头材质 W9Mo3Cr4V 与 SUS400C 热物理参数. 由表 5 可见，不锈钢的比热容比高速工具钢大，而其热传导性比高速工具钢低，因此在采用相同的焊接参数条件下，高速工具钢各测温点温度均较不锈钢搅拌头相应测温点的温度高. 由此可见搅拌头材质对搅拌摩擦焊摩擦偶温度场的分布及焊接过程中的热散失具有一定的影响. 采用比热容小、热导率高的材质制作搅拌头，焊接过程中温度变化速率快，整体温度高，说明通过其散失热量较多.

表 5　两种搅拌头材料的热物理参数

Table 5　Thermal physical parameters of W9Mo3Cr4V and SUS400C

搅拌头材质	比热容 c/(J·kg^{-1}·K^{-1})　温度 T/℃			热导率 λ/(W·m^{-1}·K^{-1})　20
	100	200	300	
W9Mo3Cr4V	482	486	515	28.4
SUS400C	494	502	519	16.0

5　结　论

(1) 搅拌摩擦焊初始阶段，搅拌摩擦区域金属的软化致使搅拌头与试板之间摩擦产热量降低，因此在搅拌头轴肩接触试板之前，搅拌头温度未能持续升高，甚至搅拌头外缘靠近轴肩区域的温度还出现一定程度的回落.

(2) 搅拌摩擦焊稳定焊接阶段，摩擦偶之间摩擦产生并传递至搅拌头的热量与通过其散失的热量处于动平衡状态，搅拌头的温度波动较小. 高速旋转的搅拌头与周围空气进行强烈的对流和辐射热交换，通过其外缘散失的热量较多，搅拌头同一测温平面上，呈现从轴线向外缘温度递减的分布特征.

(3) 搅拌头材质的热物理性能对其温度场的分布具有一定的影响，采用比热容小、热导率高的材质制作搅拌头，有利于搅拌摩擦焊过程中热量的散失.

参考文献：

[1] Salem H G, Reynols P, Lyons J S. Microstructure and retention of super plasticity of friction stir welded super plastic 2095 sheet [J]. Scripta Materialia, 2002, 46: 337 – 342.

[2] Chen C M, Kovacevic R. Finite element modeling of friction stir welding-thermal and thermomechanical analysis [J]. International Journal of Machine Tools & Manufacture, 2003, 43: 1319 – 1326.

[3] Upadhyay P, Reynolds A P. Effects of thermal boundary conditions in friction stir welded AA7050-T7 sheets [J]. Materials Science and Engineering A, 2010, 527: 1537 – 1543.

[4] 王大勇，冯吉才，王攀峰. 搅拌摩擦焊接热输入数值模型 [J]. 焊接学报，2005，26(3)：25 – 28.
Wang Dayong, Feng Jicai, Wang Panfeng. Numerical model of heat input from rotational tool during friction stir welding [J]. Transactions of the China Welding Institution, 2005, 26(3): 26 – 28.

[5] Chao Y J, Qi X, Tang W. Heat transfer in friction stir welding–experimental and numerical studies [J]. Journal of Manufacturing Science and Engineering, 2003, 125(1): 138 – 145.

[6] 李红克，史清宇，赵海燕，等. 热量自适应搅拌摩擦焊热源模型 [J]. 焊接学报，2006，27(11)：81 – 85.
Li Hongke, Shi Qingyu, Zhao Haiyan, *et al*. Auto-adapting heat source model for numerical analysis of friction stir welding [J]. Transactions of the China Welding Institution, 2006, 27(11): 81 – 85.

[7] 鄢东洋，史清宇，吴爱萍，等. 搅拌摩擦焊接过程的试验测量及分析 [J]. 焊接学报，2010，31(2)：67 – 70.
Yan Dongyang, Shi Qingyu, Wu Aiping, *et al*. Measurement and analysis of friction stir welding [J]. Transactions of the China Welding Institution, 2010, 32(2): 67 – 70.

[8] Mishra R S, Ma Z Y. Friction stir welding and processing [J]. Materials Science and Engineering R, 2005, 50, 1 – 78.

[9] 何建军，刘明宇，杨宗辉. 搅拌头 – 搅拌摩擦焊的心脏 [J]. 电焊机，2004，34(1)：24 – 27.
He Jianjun, Liu Mingyu, Yang Zonghui. Stirring head-the heart of friction stir welding [J]. Electric Welding Machine, 2004, 34

(1): 24 – 27.

[10] Hwang Yeongmaw, Kang Zongwei, Chiou Yuangcherng, *et al*. Experimental study on temperature distributions within the workpiece during friction stir welding of aluminum alloys [J]. International Journal of Machine Tools & Manufacture, 2008, 48: 778 – 787.

作者简介: 李敬勇,男,1963 年出生,博士,教授. 主要从事新材料、有色金属及异种金属连接技术、新型焊接技术研究. 发表论文40余篇. Email: jingyong_li@126.com

[上接第 26 页]

microstructure [J]. Materials Characterization, 1999, 42(1): 31 – 44.

[6] Lesnjak A, Tusek J. Processes and properties of deposits in electrospark deposition [J]. Science and Technology of Welding and Joining, 2002, 7(2): 391 – 396.

[7] 张 平,马 琳,梁志杰,等. 便携式电火花沉积镍基合金工艺 [J]. 焊接学报, 2011, 32(4): 32 – 36.
Zhang Ping, Ma Lin, Liang Zhijie, *et al*. Technique of nickel based alloy coating produced by hand electric-spark depositing process [J]. Transactions of the China Welding Institution, 2011, 32(4): 32 – 36.

[8] Gao Wei, Li Zhengwei. Nano-structured ally and composite coatings for high temperature applications [J]. Materials Research, 2004, 7(1): 175 – 182.

[9] 陈钟燮. 电火花表面强化工艺 [M]. 北京: 机械工业出版社, 1987.

作者简介: 韩红彪,男,1971 年出生,副教授,硕士研究生导师. 主要从事电火花沉积、数控技术、工业自动化设备方面的科研和教学工作. 发表论文20余篇. Email: lyhhb7157@163.com

posite using Cu-25Sn-10Ti filler alloy. The interfacial microstructure of joint was analyzed and its formation mechanism was discussed, and also the impact of interfacial microstructure on shear strength of joints at different holding time was studied. Results show that continuous interfacial reaction layer has been formed at both sides of the base materials at brazing temperature 880 ℃ and holding time for 15 min, while the typical interfacial microstructure was Invar alloy/Fe_2Ti + Cu(s,s) + (Ni, Fe, Cu)$_2$TiSn/Cu(s,s) + $Cu_{41}Sn_{11}$ + CuTi/TiSi + Ti_2O_3/SiO_{2f}/SiO_2 composite. Holding time increasing would enlarge the thickness of TiSi Ti_2O_3 layer near SiO_{2f}/SiO_2 composite, and Fe_2Ti particles would turn into blocks. The shear strength of joint would also change with increasing of holding time. The shear strength of the joints reaches a maximum of 11.86 MPa when the temperature is 880 ℃ and the holding time is 15 min.

Key words: SiO_{2f}/SiO_2 composite; Invar alloy; brazing; interfacial microstructure; shear strength

In-situ observation of cracking in wollastonite coatings and effect of powder size on fracture WANG Lubin, WANG Weize, CHEN Yufan, XUAN Fuzhen (Key Laboratory of Pressure Systems and Safety, Ministry of Education, East China University of Science and Technology, Shanghai 200237, China). pp 57 – 60

Abstract: Fracture analysis of coatings has an important role on the investigation of coating's failure mechanism, the optimization of the processing parameters and the design. The fracture of plasma sprayed wollastonite coatings was observed in-situ by using a scanning electron microscope (SEM) during the tapered double cantilever beam (TDCB) specimens were pulled open. Additionally, the effect of powder size on the coating's fracture toughness is investigated based on the observation of the microstructure, fracture morphology and cracking propagation of coatings. It was found that the cracking path was mainly influenced by the applied stress. The original pores in the coatings, including the large pores, cracks and non-bounded interfaces could guide the cracking somewhat. The fracture toughness of coatings increased and fracture paths were more curved with the decreasing of powder size

Key words: coating fracture; in-situ observation; wollastonite; plasma spraying

Linear cumulative damage analysis of welded joints under combined cycle fatigue ZHANG Tao, WANG Dongpo, DENG Caiyan, WU Liangchen (School of Material Science and Engineering, Tianjin University, Tianjin 300072, China). pp 61 – 65

Abstract: 16Mn steel welded joints are tested to fail under low cycle fatigue, high cycle fatigue and combined cycle fatigue using an apparatus that is capable of providing interactive loading. A linear cumulative damage theory is used to estimate the fatigue life of the butt joints. The proportion of each of the two fatigue load components which cause the cumulative damage is calculated. The research indicate that high cycle fatigue loads and low cycle fatigue loads simply calculated as proportion would seriously underestimate the coupling between the two components of the fatigue load when we use Miner rule to calculate the fatigue cumulative damage of specimens. However, we can take into account of the coupling between the high and low cycle fatigue loads when we turn to the outsourcing envelope of the low cycle fatigue loads.

Key words: welded joints; combined cycle fatigue; linear cumulative damage

Characteristic of temperature distributions in stirring tools during friction stir welding LI Jingyong, ZHAO Yangyang, KANG Xiaoliang (Advanced Welding Technology Provincial Key Laboratory, Jiangsu University of Science and Technology, Zhenjiang 212003, China). pp 66 – 70

Abstract: The temperature distribution in stirring tools was measured by experimental method. It is shown that the characteristic of temperature distribution in stirring tools is much different from that in workpieces. At the beginning stage of friction stir welding, the softening in stirring zone reduces the friction coefficient and the friction heat between the stirring pin and the workpiece, so the temperature in stirring tools stops rising, whereas decreases in the exterior margin of the tool before the shoulder touches the workpiece. At the steady welding stage, equilibrium exists between the heat quantity delivered to and dissipated through the stirring tool, and its temperature keeps little fluctuation. The surface of the high-speed rotating tool has intensive heat exchange with the air around it, so the temperature near its axis is higher than that on the exterior margin. The stirring tools made of metal with lower specific heat capacity and higher coefficient of heat transfer lead to heat within the welding area dissipating faster.

Key words: friction stir welding; stirring tool; temperature field

A novel composite control strategy for plasma cutting power supply based on arc control SUN Qiang, CHEN Long, CHEN Guitao, WANG Huamin (Automation & Information Engineering College, Xi'an University of Technology, Xi'an 710048, China). pp 71 – 75

Abstract: This paper analyzes static characteristics of plasma arc with the derivation of plasma arc mathematical model according to the application of low-frequency(LF) pilot arc technology in the plasma cutting power supply, and integrates with the control requirements in low-frequency(LF) pilot arc, arc transferring and arc energy transferring, and proposes a novel composite control strategy. In order to meet the power's control requirements of rapidity and stability with the load of low-frequency(LF) pilot arc, the inner loop of this strategy builds up voltage loop composite control with feed-forward arc voltage and feedback arc voltage, and the current outer loop controls the energy of plasma arc, forming a control method of feed-forward composite control of double closed-loop. Simulations and experiments were given to verify that the mentioned control strategy not only improved system's stability and robustness, but also had excellent dynamic responsibility. The power had well non-liner resilience, meeting requirements for plasma cutting power supply.

Key words: plasma cutting power supply; arc control;